EUROPEAN ORGANIZATION FOR NUCLEAR RESEARCH

CERN–PPE/91–235
18 November 1991

A FAST RICH DETECTOR FOR PARTICLE IDENTIFICATION IN THE 0.7 TO 3 GeV/c RANGE FOR LHC HEAVY-ION COLLISIONS

E. Nappi, INFN, Bari, Italy
G. Paic, GSI Darmstadt, Germany, and IRB, Zagreb, Croatia, Yugoslavia
F. Piuz, CERN, Geneva, Switzerland
R.S. Ribeiro, INIC, Coimbra, Portugal, and CERN, Geneva, Switzerland

Abstract

Based on recent test results, we present the performance of a compact fast Ring Imaging Cherenkov (RICH) detector in separating electrons, muons, pions, and kaons at $0.7 < p < 3.0$ GeV/c in view of a possible application at the Large Hadron Collider (LHC) operating in the nucleus–nucleus collision mode. The apparatus under discussion uses a solid (or liquid) radiator, and a low-gain multiwire proportional chamber (MWPC) with a two dimensional pad readout as a photoelectron detector.

Presented at the 5th Pisa Meeting on Advanced Detectors,
Isola d'Elba, Italy, 26–30 May 1991

1 INTRODUCTION

The Large Hadron Collider (LHC) which is under consideration to be built at CERN incorporates in its programme the study of nucleus–nucleus collisions to investigate the basic properties of QCD in strongly interacting bulk matter, at high-energy densities [1].

The complexity of the theoretical predictions, as well as their ambiguities related to the general problems of non-perturbative QCD requires detectors for these studies to be versatile and multi-observable. At the LHC energies ($\sqrt{s} = 6.3$ TeV per nucleon), the physics that can be studied is both soft ($p_T \leq 2$ GeV/c) and hard physics. The soft physics part puts requirements on the detectors which can be summarized as follows:

- momentum resolution ($\Delta p/p < 0.01$),
- good tracking efficiency,
- good primary and secondary vertex reconstruction efficiency,
- particle identification for $p_T \leq 2$ GeV/c in a large acceptance ($\Delta y > 1$).

Acording to the above requirements, the detector has to incorporate three main elements:

- a tracking device in the magnetic field to determine the momentum of particles, and the primary and secondary vertices,
- a particle identification (PID) device for the low-momentum range 50–700 MeV/c,
- a PID device for the upper momentum range $700 < p < 3000$ MeV/c.

In the present paper, we shall give details of the PID device for the high-momentum range for which we propose to use a fast RICH detector [2].

2 THE DETECTOR CONCEPT

The proposed detector results from a prototype test of a fast RICH detector, using as a photon detector a thin multiwire proportionnal chamber (MWPC) with a two-dimensional pad-structure read out by means of VLSI electronics [3,4]. The detector is based on the detection of UV photons emitted in a radiator medium under an angle θ_C satisfying the relation:

$$\cos\theta_C = 1/\beta n \ , \tag{1}$$

where n is the index of refraction of the medium. From Eq. (1), it follows that for the low-momentum range, the radiator medium has to have a rather large n (> 1.2), significantly narrowing the choice of available media that satisfy the refractive index requirements as well as other criteria such as UV transparency, dispersion, etc. [5].

The most convenient media are the solid sodium fluoride (NaF), and liquid Freon (C_6F_{14}).

2.1 The radiator

In table 1, we list the main physical performances and parameters which are associated with the two radiator materials of interest, NaF and liquid Freon C_6F_{14} of 10 mm thickness. The parameters are also quoted for quartz, since this material has to be used as a window in the detector assembly.

Let us recall that, in the case of normal track incidence and for quartz only, the total reflection imposes an upper limit for the emission of Cherenkov photons at the particle velocity β. The maximum momentum values are also quoted in this case.

2.2 The detector geometry

The detector geometry will be of the 'proximity focusing' type as shown in fig. 1.

This configuration has a geometry suited to achieve a very compact detector array with a minimum amount of matter. Its main components, shown in fig. 1, are the following:

- a thin radiator medium of about 20 mm thickness, including the quartz containment vessel in the case of a liquid radiator,
- a 30–70 mm UV transparent gap (nitrogen) for widening the Cherenkov photon trajectories and obtaining large Cherenkov ring radii (about 10 cm),
- a thin photon detector separated from the radiator medium by an UV transparent window (quartz).

3 MAIN TEST RESULTS OF A FAST RICH STRUCTURE

We report here the main results obtained with a prototype structure. More detailed descriptions of set-up, electronics, results, and models are available in Refs. [3] and [4].

3.1 Detector

According to the structure shown in fig. 1, the prototype consisted of:

- a radiator of 10 mm thick NaF,
- an adjustable gap, 0 to 70 mm, filled with helium,
- a quartz window (Suprasyl 2), 3 mm thick,
- the upper MWPC cathode made of a stainless steel mesh of 500 μm square, 50 μm wire, pressed against the quartz,
- 2 mm away, the sense wire plane: 20 μm diameter, 4 mm spacing, 400 mm long, raised to high voltage and all read out,
- 2 mm away, the pad cathode, with a pad size of 8×8 mm^2; an area of 12×12 pads was equipped with electronics (144 pads).

The gas used was a mixture of 95% methane and 5% isobutane passing through a tetrakis(dimethylamine)ethylene (TMAE) bubbler.

It was possible to adjust the temperature of the whole detector and the gas mixture supply up to 70 °C.

The pad electronics was composed of:

- a front-end chip, AMPLEX: 16 channel VLSI CMos including preamplifiers, filter, and analog multiplexing switches [6],
- a readout, including an 8-bit flash ADC and allowing zero suppression and pedestal subtraction at a multiplexing rate of 1 MHz [7].

The minimum sensitivity of this chain corresponds to an input charge equivalent to about 5000 electrons.

The integrating time of the front-end amplifiers is 600 ns, allowing for about 500 ns to make the decision of taking an event.

3.2 Experimental results

3.2.1 Number of detected photoelectrons per ring

Figure 2 shows the evolution of the number of photons passing through the detector for the case of normal-track incidence. From a model calculation [4], we indicate the influence of the various sources of losses when the photons propagate towards the MWPC. Since the quantum efficiency of TMAE is also taken into account, the ordinate finally represents the number of detected photoelectrons per ring. This is evaluated as a function of β.

We indicate the experimental results obtained with a TMAE temperature of 50 °C and a MWPC voltage of 1750 V. Under these conditions, the detection efficiency for single electrons was about 68%. It was observed [4] that this low-gain operation (1–2×10^4) allows us:

- a sufficient number of detected photoelectrons per ring,
- an operation without observable photon feed-back in this MWPC geometry,
- a good simultaneous detection of the associated charged particle,
- a safe and stable operation of the detector.

3.2.2 Discrimination between a minimum ionizing particle and a single photoelectron

Figure 3 shows the mean number of pads hit at the passage of a minimum ionizing particle (MIP). This number is small enough to obtain a good separation between the particle signal and the single-electron signals of the associated ring. Since the particles have a large signal due to the amount of primary ionization deposited, they can be separated from the single-electron signals in a large fraction of events. A resolution of 250 μm r.m.s. was measured for the localization of normal incidence tracks using a centroid determination [8].

3.2.3 Ring-radius resolution

The problem is to evaluate how much the pad size contributes to this resolution compared with other error sources.

In fig. 4 we show the calculation of the ring accuracy as a function of the number of detected photoelectrons per ring in the following situations:

- A1) the contribution of the radiator thickness and MWPC geometry *assuming no localization error in the detection*, i.e. the intrinsic error of the proximity focusing geometry,
- A2) localization of every photoelectron by using a centroid finding method with 8×8 mm^2 pads,
- A3) calculation of the ring radius by taking the average of all distances from the ring centre to the centre of every hit pad in a ring, (same pad size),
- B) same as (A3) but with a pad size of 4×4 mm^2.

From this calculation, we see that the dominant factor comes from the geometrical contribution, and increasing the number of pads by a factor of 4 does not provide a significant improvement.

In fig. 5a we show a measured distribution of ring radii, using the radius determination indicated under (A3), and in fig. 5b a comparison between measurements taken at different β values and the previous calculations. These results will be used later on in the discussion about the separation power.

3.2.4 Refractive index and chromaticity

The following effect has been found to be an important issue in the evaluation of the separating power of a solid radiator. The particle velocity determines a maximum index value below which photons can escape from the radiator medium without being totally reflected. That is $n_{\mathrm{TR}} = (1 + 1/\beta^2)^{1/2}$. But, the NaF index has values close to

$\sqrt{2}$ at high photon energies, taking into account its high chromatic dispersion. Hence, the most energetic fraction of the Cherenkov radiation is expected to be cut off when β approaches unity. As shown in Ref. [4] and fig. 6, this results in a decrease of the 'effective' NaF index with particle velocity and reduces the separation power for large β. In fact, this effect also contributes to the ring-radius resolution, as seen in fig. 5b. In the case of a liquid Freon radiator, these effects, which are particle-velocity dependent, are absent since the refractive index is significantly smaller than $\sqrt{2}$.

4 SEPARATING POWER

According to the previous calculations and experimental results, we show in fig. 7 the expected separation of electrons, muons, pions, and kaons that could be achieved with a NaF radiator, 10 mm thick.

The helium gap was chosen such that rings of $\sim$ 100 mm radius are generated at $\beta = 1$. The ring resolution (one standard deviation), measured at different β values (fig. 5b), is indicated, providing an eye evaluation of the separations. In fig. 8, we show the performances calculated with a freon radiator, 10 mm thick.

In both cases, the kaon identification is straightforward within the momentum range of interest, even close to threshold, despite the decrease of the number of photoelectrons per ring, as shown in fig. 9a and b. Protons should be mostly identified from the lack of ring and, possibly, from a high level of ionization signal. We also show in the enlargement in figs. 7 and 8 the interesting possibility of separating electrons from muons and pions up to about 0.8 GeV/c.

5 THE RICH DETECTOR IN THE LHC ENVIRONMENT

The planning of the exact size of a RICH detector in the LHC experimental area is difficult because, at the present time, considerable uncertainty remains on the projected multiplicities of charged particles at mid-rapidity. The prediction varies from 2000 up to 8000 per unit of rapidity. A large rapidity density requires the building of a detector with a larger radius, and hence a larger surface, to achieve an acceptable pattern recognition.

At present, experiments using RICH detectors (DELPHI [9], NA35 [10], etc.) consider a particle density of about 40/m^2 to be an acceptable limit.

To compare this figure with the above-mentioned rapidity density, one has to bear in mind several facts:

– the MWPC has a capacity of distinguishing single photon hits from impact of MIPs,
– particles entering the RICH detector with energies below the threshold will result only in the easily identifiable points of impact created by ionization.

Taking into account the above remarks and the mean momenta of pions, kaons, and protons, we can estimate at 65–70% the fraction of particles that yield recognizable rings.

Starting with the maximum rapidity density predicted, we have to deal with ring densities of 40/m^2 at 4.5 m from the colliding beams. This is a ring density deemed manageable by the simulations and existing experimental results.

It should be noted that the RICH detector would also help to resolve the problem of electrons interfering with the dE/dx measurement in the 100–1000 MeV/c range.

6 CONCLUSIONS

We have presented a fast RICH detector that could operate in the LHC environment at the rate of about 100 Hz, which would be compatible with an overall 10^4 Hz collision rate in the collider for the nucleus–nucleus mode at $\mathcal{L} = 2 \times 10^{27}$ cm^{-2} s^{-1}.

The low amplification necessary in the MWPC for a sufficiently high output signal makes this type of UV photon detector rather immune to photon feedback, sparking, and other sources of noise.

Below, we summarize the main characteristics of the proposed detector:

- range e/π : < 0.8 GeV/c
- range μ/π : < 0.6 GeV/c
- range π/K: < 3.5 GeV/c
- range K/p: < 7 GeV/c or no ring
- sensitivity to a $\Delta p/p$ of 2%: low
- directional sensitivity: large, necessitates good tracking
- impact point determination: < 250 μm
- two-track separation: < 10 mm
- thickness in radiation length: 30–35%
- thickness in interaction length: 10–12%
- admissible density of hits: 30–40/ m^2
- event rate: 10 kHz
- data-acquisition rate: 100 Hz
- modularity: high
- radial compactness: 150 mm.

ACKNOWLEDGEMENT

One of us (G.P.) acknowledges the support of the Commission of the European Communities.

REFERENCES

[1] Proc. Large Hadron Collider Workshop, CERN 90–10 (1990), Vol. 2.
[2] R. Arnold et al., Nucl. Instrum. Methods **A273** (1988) 466.
[3] F. Piuz et al., Nucl. Instrum. Methods **A283** (1989) 602.
[4] F. Piuz et al., preprint CERN–PPE/91–7 Rev., presented at the Conference on Experimental Apparatus for High Energy Particle Physics and Astronomy, San Miniato, Italy, 1990.
[5] J. Seguinot, preprint CERN–PPE/89–92, and LPC 89–25 (1989).
[6] E. de Beuville et al., Nucl. Instrum. Methods, **A288** (1990) 157.
[7] E. Chesi et al., CERN/ECP Internal note about DRAMS, 1990.
[8] F. Piuz et al., CERN/PPE, Internal OMD note, Pad MWPC at Omega, 1991.
[9] DELPHI barrel RICH group, private communication.
[10] G. Paic and NA35 Collaboration, Contribution to Quark Matter 91
Proc. 9th Int. Conf. on Ultra-relativistic Nucleus–Nucleus Collisions, Gatlinburg, TN, USA, 1991.

Table 1
Main physical performances of radiators

	C_6F_{14} (Liquid Freon)	NaF (Solid)	Quartz (Solid)
Refractive index at 180 nm	1.28	1.39	1.57
β at Cherenkov threshold ($= 1/n$)	0.78125	0.7194	0.63694
β at total reflexion ($= 1/\sqrt{(n^2-1)}$	none	partial	0.8262
Maximum Cherenkov angle ($\beta = 1$) [°]	38.62	44.0	50.43
Maximum opening angle in helium at $\beta = 1$ [°]	53.03	74.89	Total reflection
Cherenkov threshold(s)			
for muons [MeV/c]	132	109	87–105
for pions [MeV/c]	174	144	115–205
for kaons [MeV/c]	617	511	407–724
for protons [MeV/c]	1174	972	775–1376
Number of Cherenkov photons per cm at $\beta = 1$	144	178	220
Radiation length [mm]	138	117	123
Interaction length [mm]	420	381	376

Fig. 1 Scheme of a fast RICH layout with a proximity focusing geometry.

Fig. 2 Cumulative effect of the sources of photon losses after: 1–transmission, 2–total reflection, 3–reflection, 4–transmission through the mesh cathode, 5,6,7–TMAE absorption at 50, 40, and 30 °C. In order to have the ordinate unit as a number of electrons, all curves include the TMAE quantum efficiency and a detector efficiency for single electrons of 68%. Full circles are measurements with TMAE at 50°C, 1750 V, single-electron detection efficiency of 68%.

Fig. 3 a) Dependence of the mean number of pads hit per MIP inside (open symbol) and outside (full symbol) the central zone as a function of TMAE temperature and chamber gain. Square: 1750 V, circle: 1800 V, pion $\beta = 0.995$. b) Scheme of the central 'beam' zone.

Fig. 4 Simulated dependence of the resolution of the ring radius as a function of number of photoelectrons detected per ring. a) pad size: 8×8 mm^2, b) pad size: 4×4 mm^2.

Fig. 5 a) Distribution or ring radii. Protons $\beta = 0.966$, TMAE at 40°C, HV = 1750 V. The mean radius is 36.40 mm. b) Ring resolution. Open symbols: calculated with NaF (circle) and liquid Freon (square). Full symbols: measured with NaF.

Fig. 6 Simulation of the variation of the mean index of NaF as a function of β when all mechanisms of photon losses are taken into account within the wavelength range of 150–220 nm. Also shown is the influence of the mean free path of photoabsorption in TMAE of 4, 7, and 12 mm (triangle, circle, square).

Fig. 7 Separating power with a NaF radiator of 10 mm thickness. The error bars are taken as the measured ring resolutions (one standard deviation).

Fig. 8 Separating power with a liquid Freon radiator of 10 mm thickness. The error bars are taken as the calculated ring resolutions (one standard deviation).

Fig. 9 a) Mean number of photoelectrons per ring as a function of momentum for different particles. NaF radiator, 10 mm thickness. b) Ring-radius resolution as a function of momentum for different particles. NaF radiator, 10 mm thickness.

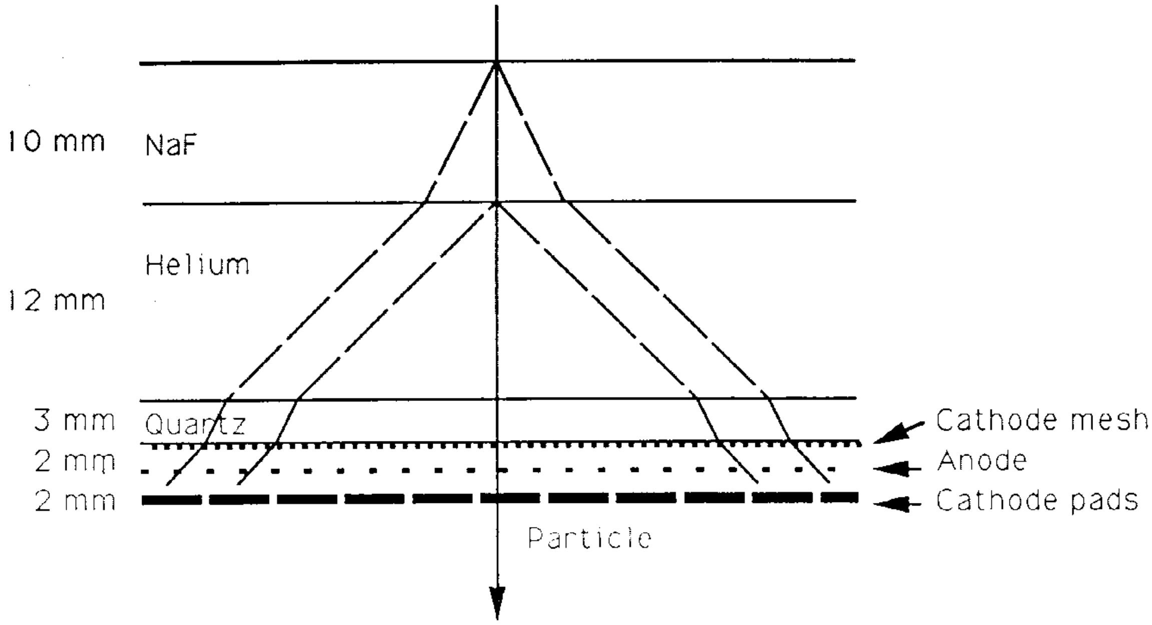
10 mm
NaF
Helium
12 mm
3 mm
Quartz
2 mm
2 mm
Cathode mesh
Anode
Cathode pads
Particle

Fig. 1

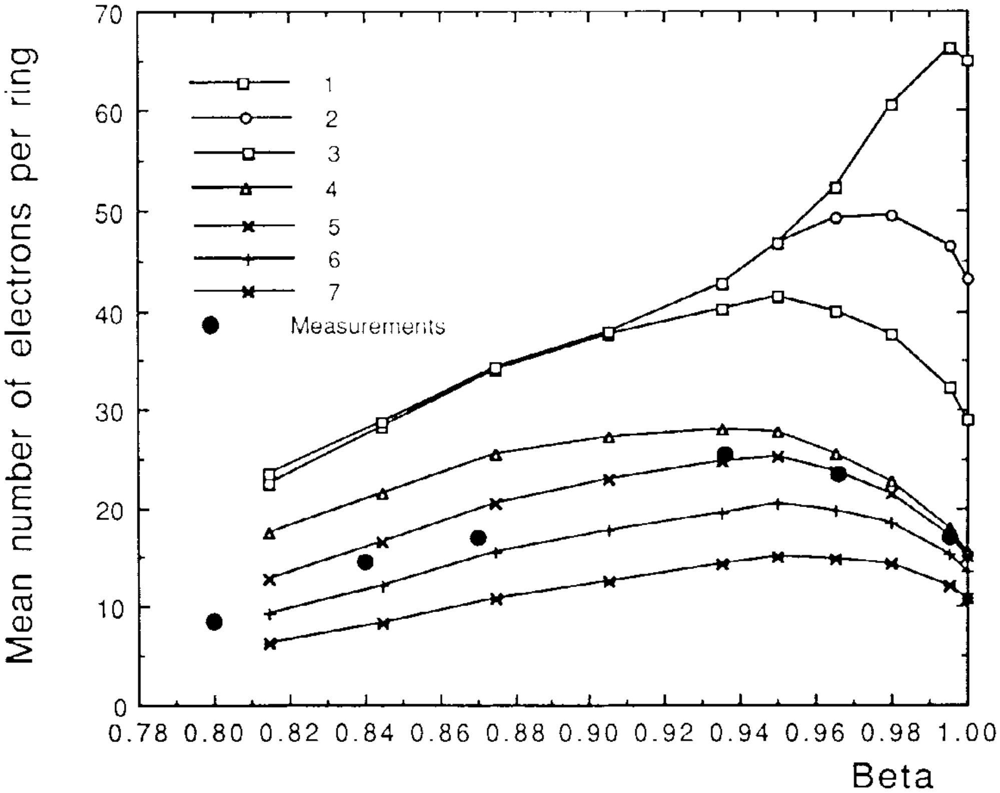
Mean number of electrons per ring
Beta
0
10
20
30
40
50
60
70
0.78 0.80 0.82 0.84 0.86 0.88 0.90 0.92 0.94 0.96 0.98 1.00
1
2
3
4
5
6
7
Measurements

Fig. 2

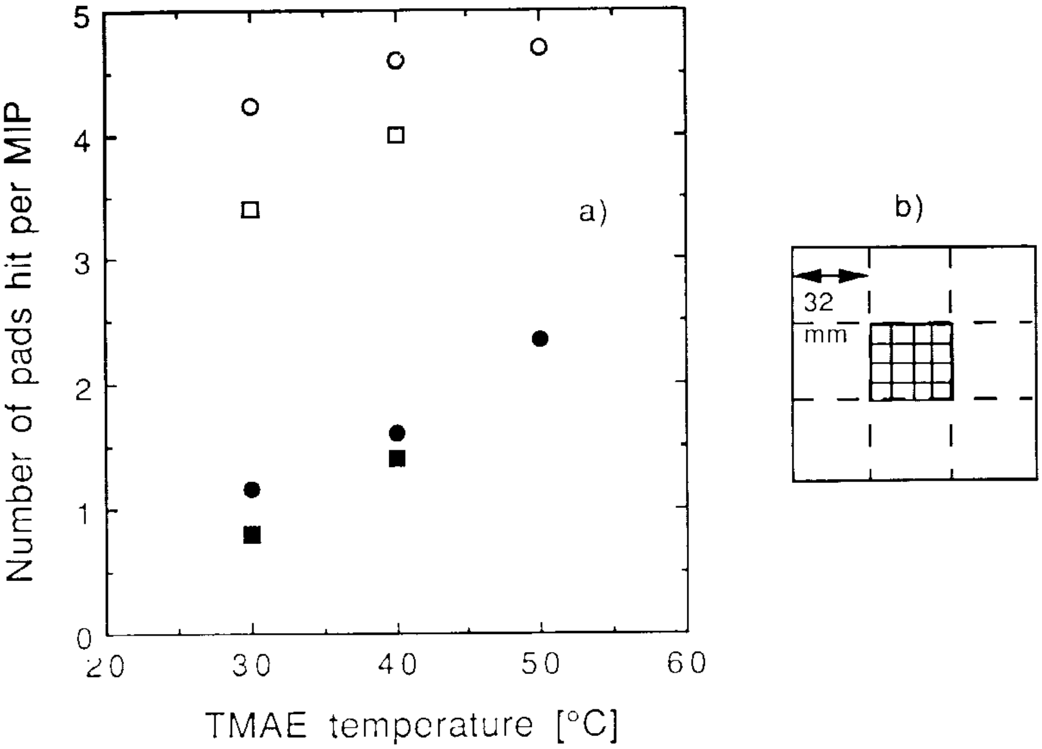

Number of pads hit per MIP
5
4
3
2
1
0
20
30
40
50
60
TMAE temperature [°C]
a)
b)
32
mm

Fig. 3

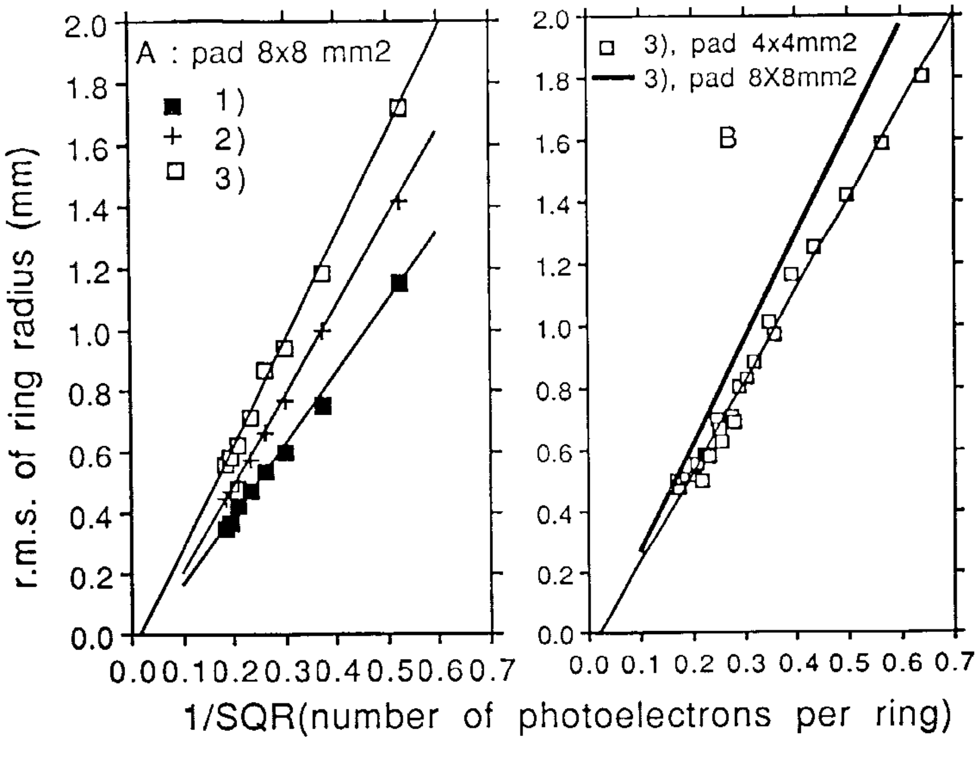

r.m.s. of ring radius (mm)
A : pad 8x8 mm2
1)
2)
3)
3), pad 4x4mm2
3), pad 8X8mm2
B
2.0
1.8
1.6
1.4
1.2
1.0
0.8
0.6
0.4
0.2
0.0
0.00.10.20.30.40.50.60.7
0.0 0.1 0.2 0.3 0.4 0.5 0.6 0.7
1/SQR(number of photoelectrons per ring)

Fig. 4

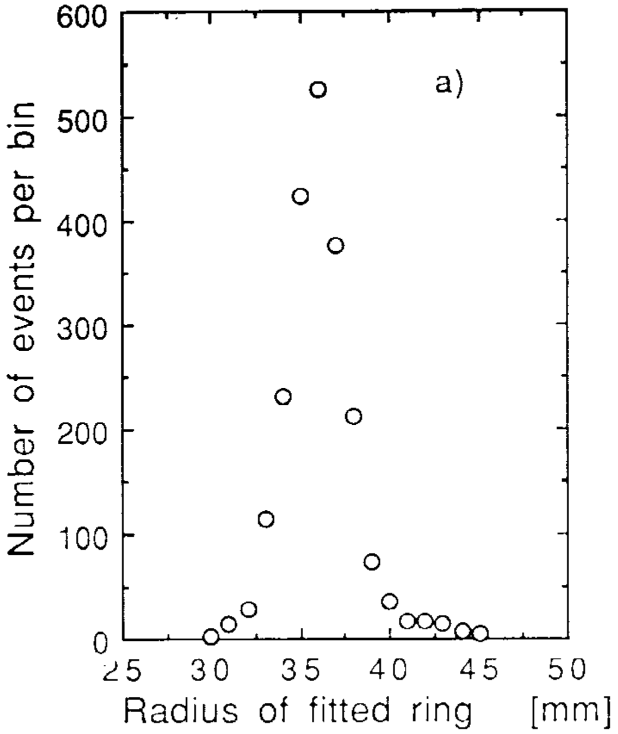

a)
Number of events per bin
Radius of fitted ring [mm]
b)
NaF calculated
NaF measured
Freon calculated
r.m.s. ring radius [mm]
Beta

Fig. 5

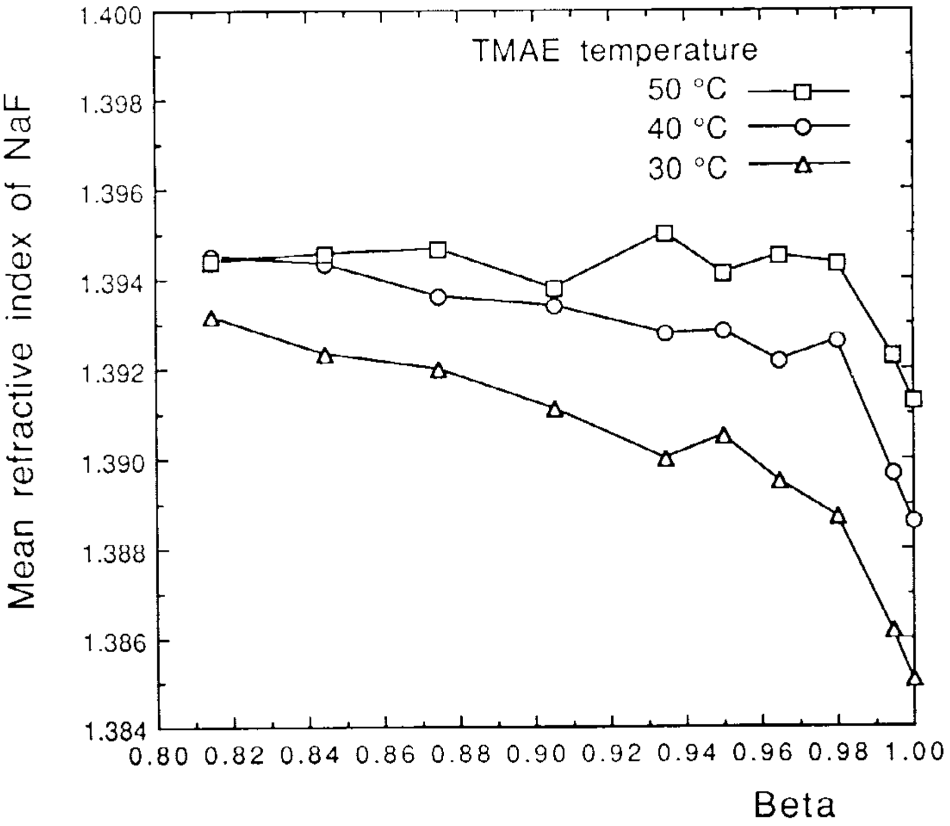

TMAE temperature
50 °C
40 °C
30 °C
Mean refractive index of NaF
Beta

Fig. 6

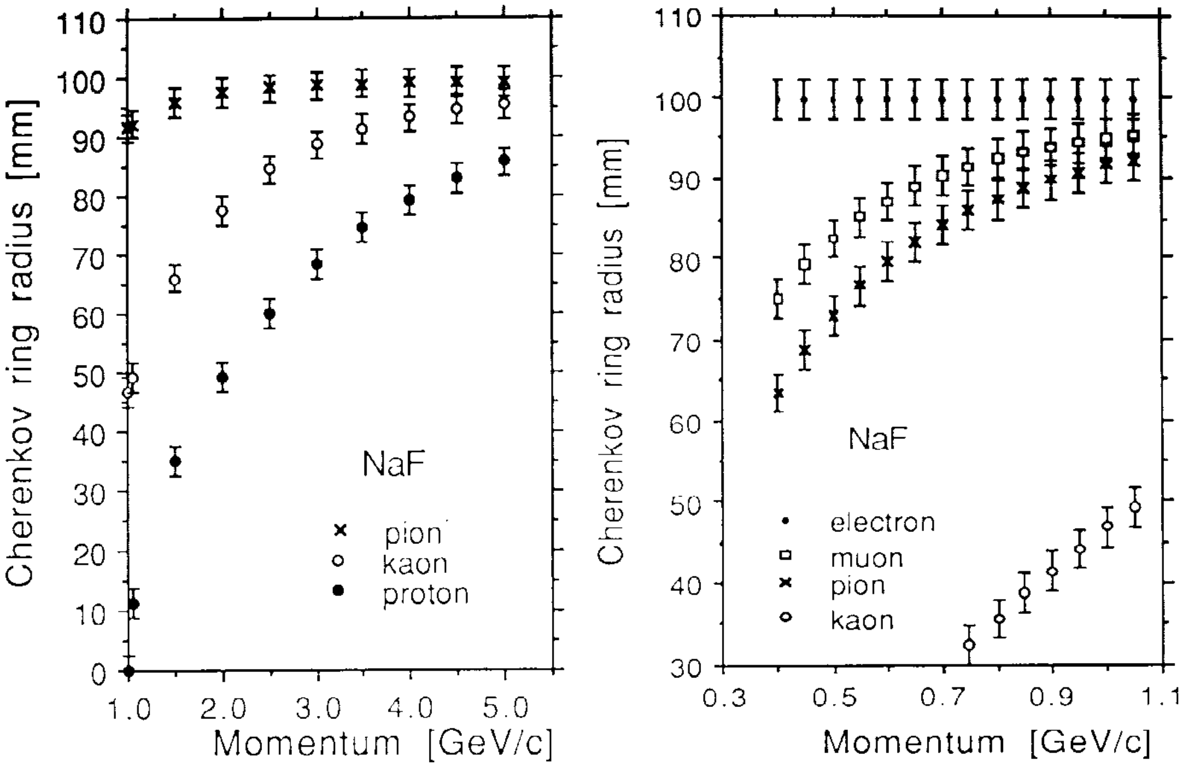
Cherenkov ring radius [mm]
Momentum [GeV/c]
NaF
pion
kaon
proton
NaF
electron
muon
pion
kaon

Fig. 7

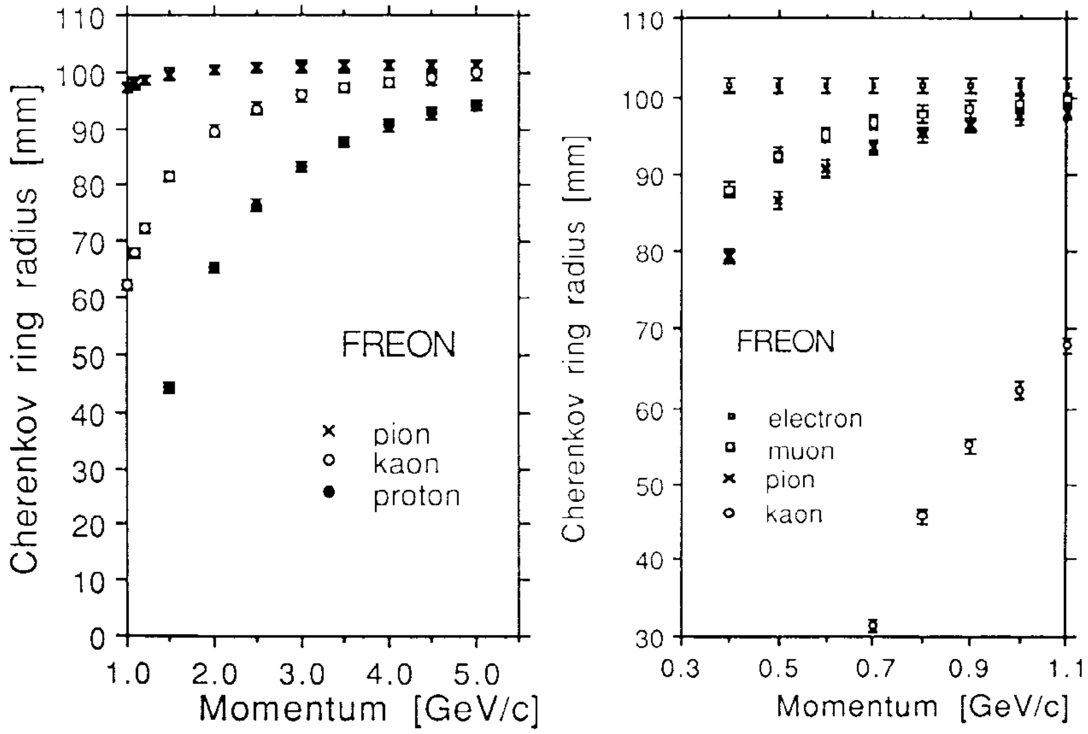
Cherenkov ring radius [mm]
Momentum [GeV/c]
FREON
pion
kaon
proton
FREON
electron
muon
pion
kaon

Fig. 8

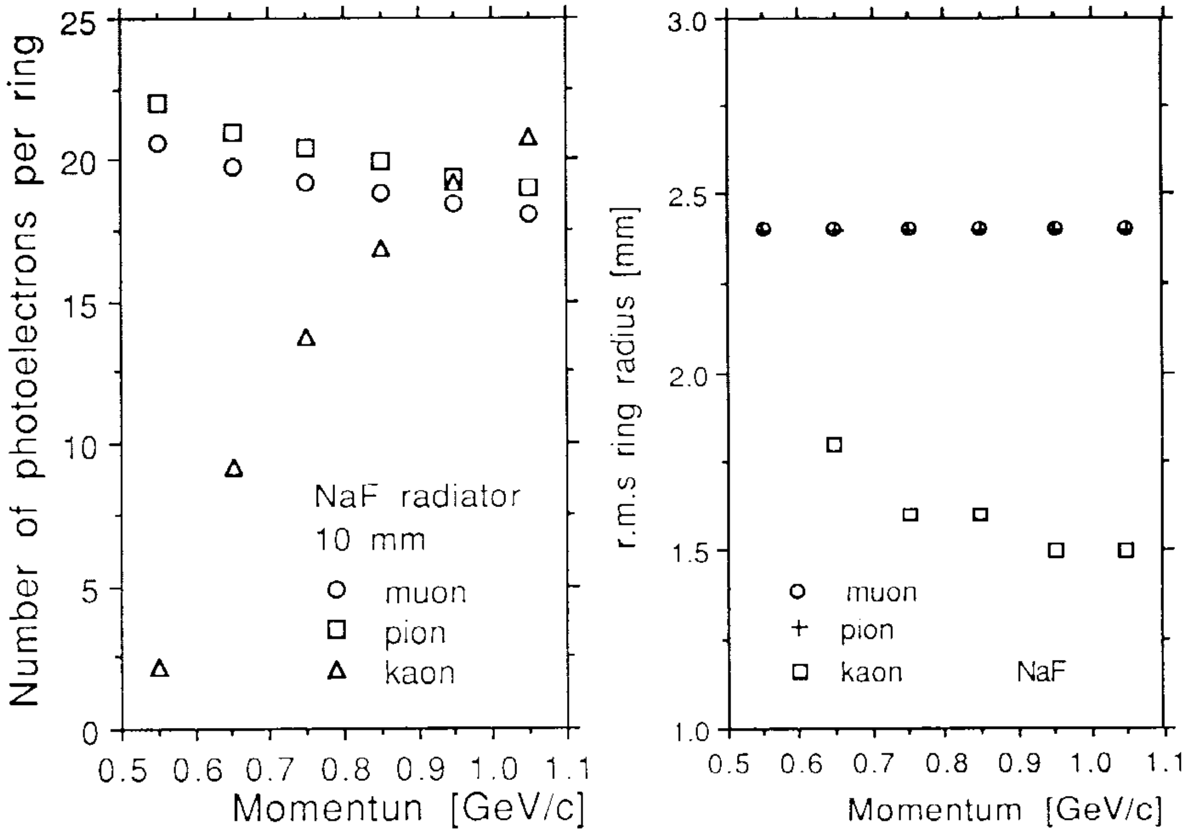

25
20
15
10
5
0
Number of photoelectrons per ring
0.5 0.6 0.7 0.8 0.9 1.0 1.1
Momentun [GeV/c]
NaF radiator
10 mm
muon
pion
kaon
3.0
2.5
2.0
1.5
1.0
r.m.s ring radius [mm]
0.5 0.6 0.7 0.8 0.9 1.0 1.1
Momentum [GeV/c]
muon
pion
kaon
NaF

Fig. 9